Revealing the Topological Drivers of Hydraulic Transients in Water Distribution Networks

Water Resources Research

RESEARCH ARTICLE
10.1029/2025WR040594

Revealing the Topological Drivers of Hydraulic Transients in Water Distribution Networks

R. Vesipa[1], **L. Ridolfi**[1], **and S. Fellini**[1]

[1]DIATI, Politecnico di Torino, Turin, Italy

Key Points:

- Flow transient simulations in pipe networks are interpreted using topological metrics obtained from complex network theory
- Topological metrics predict transient responses, with key factors like pipe count and connectivity explaining up to 90% of surge variability
- The relationship between hydraulic and topological metrics is interpreted, revealing how network structure influences transients

Supporting Information:

Supporting Information may be found in the online version of this article.

Correspondence to:

R. Vesipa,
riccardo.vesipa@polito.it

Citation:

Vesipa, R., Ridolfi, L., & Fellini, S. (2026). Revealing the topological drivers of hydraulic transients in water distribution networks. *Water Resources Research*, *62*, e2025WR040594. https://doi.org/10.1029/2025WR040594

Received 23 MAR 2025
Accepted 21 DEC 2025

Author Contributions:

Conceptualization: R. Vesipa, L. Ridolfi, S. Fellini
Data curation: R. Vesipa, S. Fellini
Funding acquisition: L. Ridolfi
Investigation: R. Vesipa, L. Ridolfi, S. Fellini
Methodology: R. Vesipa, L. Ridolfi, S. Fellini
Software: R. Vesipa, S. Fellini
Supervision: R. Vesipa
Writing – original draft: R. Vesipa, L. Ridolfi, S. Fellini
Writing – review & editing: R. Vesipa, L. Ridolfi, S. Fellini

Abstract The spatiotemporal dynamics of pressure surges is a complex phenomenon involving nonlinear mechanisms such as wave propagation, reflection, and interference. Pipe networks, in particular, pose a challenge in understanding pressure surge patterns. At each junction, where two or more pipe branches meet, an incoming pressure wave interacts with the junction, generating new forward and backward waves further complicating surge behavior. The importance of junctions in shaping pressure surges naturally raises the question of how network topology (e.g., number of junctions, number of branching pipes) influences pressure surge propagation within pipe networks. To investigate this, we conducted a flow transient analysis on a large set of synthetic lattice networks and extracted hydraulic metrics describing head variations at network junctions. We then characterized the connectivity structure of the networks using metrics derived from complex network theory. Finally, we assessed whether topological metrics alone could predict local and global hydraulic transient responses. Our findings show that many hydraulic metrics can be accurately estimated from topological metrics, with a coefficient of determination R^2 of up to 0.96. These results underscore the crucial influence of network topology on the transient behavior of pipe systems during operational maneuvers.

Plain Language Summary In water distribution networks, sudden changes in flow rate, such as those caused by the rapid opening or closing of a valve, can trigger water hammer phenomena, leading to pressure surges within the system. If not controlled, these surges can cause significant damage to the infrastructure. In this study, we investigated how the design of these networks influences the behavior of pressure surges. By analyzing various network configurations, we identified key factors, such as the number of pipes and their connections, that play a critical role in determining how pressure waves propagate through the system. Our findings demonstrate that by understanding the network's design, we can predict the severity of these pressure surges. This is crucial for engineers, as it enables them to create more resilient water distribution systems that can better withstand sudden changes in pressure.

1. Introduction

Water distribution networks (WDNs) are among the most critical infrastructures for human societies (Mala-Jetmarova et al., 2015). This importance explains why they have consistently attracted the attention of the scientific community. New technologies, innovative conceptual tools, and increasingly stringent demands from industry continuously drive the development of new solutions for the design, management, and maintenance of WDNs. At the same time, the pressing need to address water resource management challenges, such as scarcity and sustainable use, further stimulates this development.

In recent years, complex network theory (CNT, or graph theory) has emerged as a notable example of how a novel conceptual framework is influencing the study of WDNs. Originating in the mathematics and physics communities, this theory examines the relationships between the topological structure of a network and its functioning (e.g., Albert & Barabási, 2002; Boccaletti et al., 2006, 2014; M. Newman, 2018). CNT has experienced rapid development and has proven to be highly valuable in various technical and scientific domains, including turbulence (Iacobello et al., 2021; Schäfer et al., 2018), infrastructure networks (Barthélemy, 2011), and pollutant dispersion in urban environments (Fellini et al., 2021), among others (see, e.g., Costa et al., 2011 for a comprehensive survey of real-world applications). The theory has provided innovative analyses, novel metrics, and new insights into the relationships among elements interconnected within the network.

As one of the most prominent examples of infrastructure networks, WDNs have benefited significantly from these advancements, leading to numerous CNT applications (see Torres et al. (2017) and the recent review by Yu et al. (2024)). Examples include the use of CNT to characterize system domains (e.g., Giustolisi et al., 2017;

Yazdani & Jeffrey, 2012), provide the operational state (e.g., Giustolisi et al., 2019; Meng et al., 2018), assess vulnerabilities (e.g., Giustolisi et al., 2022), formulate maintenance plans (e.g., Dunn & Wilkinson, 2013), select optimal sensor placement (e.g., de Schaetzen et al., 2000; Perelman & Ostfeld, 2013), and sectorize networks (e.g., Di Nardo & Di Natale, 2011; Giustolisi & Ridolfi, 2014; Khoa Bui et al., 2020; Saleh & Tanyimboh, 2014).

In this study, we build on this line of inquiry by exploring how CNT can be leveraged to describe water hammer phenomena in WDNs. This topic remains a niche within WDN research, partly due to a prevailing belief among practitioners that the network structure leads to rapid attenuation of pressure waves (e.g., Twyman, 2018) and, consequently, a quick damping of pressure peaks induced by unsteady motion. Specifically, the simplistic assumption is that the meshed structure itself protects the network from water hammer. However, this is not the case: the complex looped topology, presence of dead ends, variations in wave celerity across pipes, and reflections at nodes can result in non-trivial interferences between forward and backward waves, potentially leading to unexpectedly high local pressure values (Meniconi et al., 2018, 2022; Starczewska et al., 2015; Vardy, 2023; Vesipa & Fellini, 2019).

These considerations indicate that the hydraulic response of networks under unsteady flow conditions is governed to a significant extent by their topological configuration and the geometric attributes of their links. It follows that CNT-based metrics, when properly tailored to reflect the pivotal role of network architecture on the propagation and interaction of pressure waves, may offer a key tool for estimating the response of a WDN to the water hammer.

A noteworthy recent contribution to this topic is the study by Marsili et al. (2023), which begins to explore the application of CNT to water hammer analysis. The authors examined how flow transients vary with changes in topology caused by valve closures, and their results highlighted that some topological metrics derived from graph theory were significantly correlated with overpressures caused by the water hammer.

Starting from these promising results, our aim is to further investigate the potential of CNT in the context of the unsteady behavior of WDNs. To this end, we generated a large ensemble of synthetically-constructed realistic networks, enabling a systematic exploration of a broad spectrum of sizes, topologies, and hydraulic characteristics that are representative of real-world systems. On such networks, we conducted simulations of the hydraulic phenomenon of water hammer, including wave propagation, reflection, interference, and friction, to obtain time series of head variations in each junctions, and scalar metrics capable to synthesize these time series. Subsequently, we evaluated a number of CNT-based metrics and examined their ability (individually and in combination) to describe the hydraulic metrics. We tested many metrics, both purely topological measures and incorporating WDN-specific weights, and applied several multivariate forecasting models. Compared to previous studies, this work advances the field in three key respects: (i) testing a substantially larger set of topological and hydraulic configurations, (ii) examining a broad range of CNT-based metrics, and (iii) integrating these metrics into nonlinear models designed to predict network overpressures.

Although exploratory in nature, our study yielded encouraging results, showing that (i) the connectivity structure, when appropriately weighted by geometric characteristics, encapsulates valuable information on network behavior under unsteady conditions, and (ii) CNT-based metrics, specifically tailored to hydraulic systems, are effective in extracting this information, particularly when employed within multivariate models that summarize the contributions of individual metrics. These findings hold substantial practical relevance, showing that a preliminary yet informative assessment of unsteady motion in a WDN can be performed without resorting to the computationally intensive simulations traditionally employed for modeling wave propagation. This approach would enable the systematic analysis of water hammer across numerous design configurations of the network (e.g., different topologies, diameter assignments, and valve closing maneuvers), reserving detailed hydraulic simulations for only a carefully selected subset of cases (e.g., Huang et al., 2017; Nault et al., 2016; Riaño-Briceño et al., 2022).

The remainder of this paper is organized as follows. Section 2 describes the types of networks considered, the hydraulic modeling approach, the numerical simulations, and the specific metrics employed (both hydraulic and CNT). Section 3 addresses how the synthetic networks were generated and their hydraulic and topological characteristics. Section 4 presents and analyzes the results, while Sections 5 and 6 discuss the findings and outline the main conclusions, respectively.

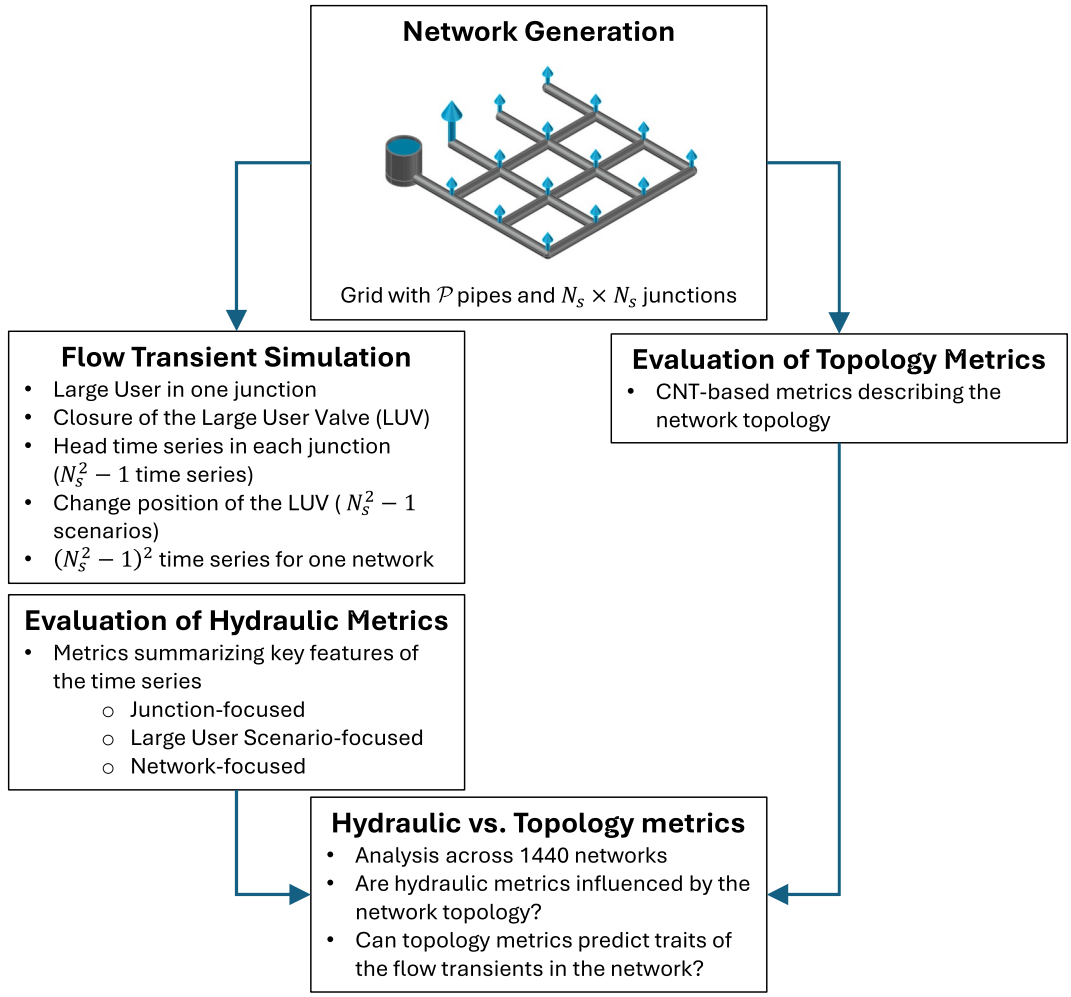

Figure 1. Flow chart of the adopted methodology.

2. Methods

In this section, we describe the methodological framework adopted in this study (see also the flow chart shown in Figure 1). First, we present the type of hydraulic networks considered (Section 2.1), followed by the hydraulic model and the numerical solution employed to simulate hydraulic transients (Section 2.2). We then introduce the hydraulic metrics used to quantify the effects of overpressures generated by water hammer within the network (Section 2.3), and the topological metrics that characterize the network's structure and geometry (Section 2.4). Finally, we detail the multiplicative correlation model employed to link the topological and hydraulic descriptors (Section 2.5).

2.1. Reference Water Distribution Network

For the sake of generality, we do not focus on a specific case study; instead, we consider a set of square, regularly gridded networks that are representative of densely populated neighborhoods. These networks incorporate typical residential demands as well as background leakages, while explicitly accounting for flow transients induced by a large user whose demand is roughly an order of magnitude higher than that of ordinary consumers (Starczewska et al., 2015). A typical example includes a hospital or a shopping mall connected to the network: such facilities may abruptly interrupt their water consumption due to rapid valve closure or operational shutdowns. This sudden change in flow can trigger significant hydraulic transients, which subsequently propagate throughout the surrounding residential network. To enable a systematic assessment, the analysis considers all possible scenarios in

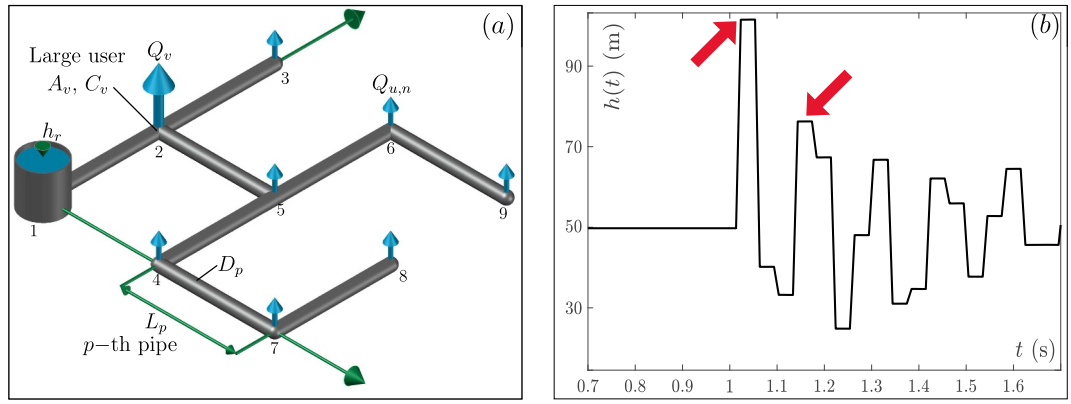

Figure 2. (a) Schematic layout of the gridded water distribution network considered in this work for the case $N_s = 3$. Blue arrows represent the water outflows at junctions. At Junction $n = 2$, the outflow of the large user, Q_v is regulated by the large user valve (LUV) with opening $A_v(t)$ and flow coefficient C_v. (b) Variations of head in a generic junction (here $n = 3$) induced by the shutting of the LUV. The red arrows mark two consecutive peaks of the head time series.

which the large user is located at different junctions in the network. This gives rise to a number of large user scenarios (LUSs) for each network.

In this context, we define a reference water distribution network (WDN) that provides the basic framework and notation for the subsequent analyses (Figure 2). The layout consists of $N_s \times N_s = N$ junctions, each identified by an index n, and where N_s is the number of junctions per side. The grid includes $\mathcal{P}$ pipes, each indexed by p and characterized by their length (L_p), diameter (D_p), wall thickness, and equivalent roughness. Pipe materials are defined by Young's modulus and Poisson's ratio. The surge wave celerity within the pipe, a_p, is determined by the pipe's geometry and material properties, as well as the water's density and bulk modulus.

A valve, called the large user valve (LUV) governs the outflow of the large user, and is installed at a single junction ($n = v$) in the network. This junction features a large pressure-driven outflow. The LUV has maximum opening A_v and flow coefficient C_v. Variations in $A_v(t)$ over time drive the hydraulic transients analyzed in this study. In particular, we will consider the case in which the outflow from the large user is completely stopped by closing the LUV. Variations of $v = 2, \ldots, n$ provide all possible LUSs considered ($N_s^2 - 1$ for each network).

At all other junctions, smaller pressure-driven outflow occur (see Figure 2), representing minor demands (residential users) or leakages from connected pipes. As it is custom in flow transient analysis (e.g., Xing & Sela, 2020) this outflows are modeled as orifices with fixed opening ($0.1 \cdot A_v$) and flow coefficient (C_v), though more sophisticated formulations (e.g., a pressure-dependent flow coefficient, May 1994) could be easily incorporated. Finally, a reservoir connected to the first junction of the lattice supplies the network and maintains a constant head, h_r. By varying the network size (N_s) and the degree of interconnection ($\mathcal{P}/N$), this reference structure can be generalized into a wide set of synthetic WDNs with diverse hydraulic and topological characteristics, as detailed in Section 3. By varying the location of the LUV, several LUSs can be considered.

2.2. Hydraulic and Numerical Model for the Water Distribution Network

Hydraulic transients in each pipe are modeled by a system of partial differential equations that describe momentum balance and mass conservation (Chaudhry, 2014)

$$\frac{\partial Q_p}{\partial t} + gA_p \frac{\partial h_p}{\partial x_p} + \mathcal{R} Q_p |Q_p| = 0, \tag{1}$$

$$a_p^2 \frac{\partial Q_p}{\partial x_p} + gA_p \frac{\partial h_p}{\partial t} = 0, \tag{2}$$

where $Q_p(x_p, t)$ and $h_p(x_p, t)$ are the flow rate and piezometric head, respectively, both varying with space and time t; x_p is the longitudinal coordinate along the pipe, oriented downstream; $A_p = \pi D_p^2/4$ is the pipe cross

section; $\mathcal{R} = f/(2D_pA_p)$ is the friction term according to the Darcy-Weisbach formulation, where f is the friction factor.

Boundary conditions reflect the physical constraints at the pipe ends. For a pipe connected to the reservoir

$$h_p(x_p = 0, t) = h_r - (1 + k_e)\frac{Q_p(x_p = 0, t)^2}{2gA_p^2}, \tag{3}$$

where $k_e = 1$ is the coefficient of entrance loss.

At junctions, in all pipes connected to the same node the equivalence of piezometric head h_n holds, that is, $h_n = h_p(x_p = L_p)$ for pipes entering the node, and $h_n = h_p(x_p = 0)$ for pipes leaving the node. In addition, the continuity equation reads

$$\sum_p Q_p^{in}(h_n) - \sum_p Q_p^{out}(h_n) - \zeta_n\sqrt{h_n - z_n} = 0, \tag{4}$$

where Q_p^{in} and Q_p^{out} are the pipe flows into and out of the node, z_n is the node elevation, and ζ_n is the effective orifice area. For $n \neq v$, ζ_n is constant over time, while for $n = v$, (i.e., for the LUV) $\zeta_n = \zeta_n(t) = C_v \cdot A_v(t)$. Variations in $A_v(t)$ over time drive the hydraulic transients analyzed in this study. A detailed explanation of how the aforementioned equations are combined to build the hydraulic model of a gridded network is reported in Supporting Information S1. The initial conditions along all pipes correspond to the steady-state flow in the WDN.

In order to solve Equations 1 and 2 with the boundary conditions (Equations 3 and 4) the method of characteristics as reported in Chaudhry (2014) is adopted. This method reduces the partial differential equations to ordinary differential equations along characteristic lines, which are then solved using a finite difference scheme. A detailed explanation of the numerical aspects adopted is reported in Supporting Information S1.

The simulations are designed to investigate how the network responds to sudden closures of the LUV at different locations. For each network and for each LUS considered in this study (see Section 3), the LUV is assumed to be installed at a selected junction $n = v$ (e.g., $v = 2$ in Figure 2a), and the network response is simulated as the LUV's opening area $A_v(t)$ is linearly reduced to zero over 0.1 s. The primary output of the simulations is the time series of piezometric head at each junction, capturing the transient effects induced by the LUV closure. The simulation duration is chosen to ensure that at least two head peaks are observed at every junction, as illustrated by the red arrows in Figure 2b.

This procedure is repeated for different LUSs, that is, relocating the LUV to a different junction in the network in each scenario, except for the reservoir junction ($n = 1$). In this way, the index v spans all possible junctions from 2 to N, allowing a systematic assessment of the network's hydraulic response to the LUV's closure, considering all possible positions of the LUV.

For each network and for each LUV location the simulations yield the time series of head and flow rate at every computational node. This huge amount of data calls for a synthesis into scalar hydraulic indicators, as presented in the following section.

2.3. Hydraulic Metrics

To characterize the severity and spatial extent of water-hammer events in the simulated WDNs, we introduce a set of scalar hydraulic metrics derived from the simulated head time series. These metrics are designed to capture both local and global features of the transient response, enabling direct comparison across different LUSs and network configurations. In particular, we focus on indicators that quantify the magnitude of overpressures at each junction and their aggregated values over the entire network.

The rationale for introducing these scalar metrics is that each junction produces a time series of pressure responses, and every possible LUS generates distinct transient dynamics. The analysis therefore yields a very large number of time series, which would be difficult to interpret without further synthesis. Several options can be pursued, and different metrics can be defined. We choose to define metrics that relate overpressures with steady-

state conditions, as head in steady-state conditions is a standard indicator used by operators. In this way, these metrics quantify deviations induced by flow transients relative to steady-state conditions, making the results both easier to synthesize and directly comparable with standard operational benchmarks.

Three levels of aggregation are considered: (i) *junction-focused* metrics, which describe the effect of a given LUV closure on individual junctions; (ii) *LUS-focused* metrics, which summarize the network-wide impact of closing a specific LUV; and (iii) *network-focused* metrics, which provide a single value representative of the entire network behavior for all possible LUSs.

We begin with the first level of aggregation (*junction-focused* metrics), analyzing the head time series at the network junctions for a specific LUV locations. Let $h_v(n,t)$ be the head at junction n when the LUV is located at junction v. Since the reservoir is fixed at $n = 1$, the analysis only considers $n = 2,3,\ldots,N$. For illustration, Figure 3a shows a network with $N_s = 3$ and $N = 9$ (as in Figure 2).

The severity of the transient at junction n is quantified by the maximum head increment relative to the steady state, normalized by the steady-state head

$$\Delta H_0(v,n) = \frac{\max_t [h_v(n,t) - h_v(n,0)]}{h_v(n,0)}. \tag{5}$$

This scalar provides a direct measure of the overpressure at each junction for a given LUS. For example, Figure 3b reports $\Delta H_0(2,n)$ for $n = 2,\ldots,9$. In a network with $N_s \times N_s$ junctions, each specific LUS (characterized by a different LUV location) yields $\left(N_s^2 - 1\right)$ values of ΔH_0.

At the second level of aggregation, the *junction-focused* metrics $\Delta H_0(v,n)$ are combined to describe the overall network response to the closure of a specific LUV. For each LUV location, two *LUS-focused* metrics are defined

$$\overline{\Delta H_0}(v) = \frac{1}{(N-1)} \sum_{n=2}^{N} \Delta H_0(v,n), \tag{6}$$

and

$$\Delta H_{0,\max}(v) = \max_n [\Delta H_0(v,n)]. \tag{7}$$

The first metric quantifies the average relative overpressure across the network, while the second captures the most severe local transient. Both depend on the considered LUS, that is, LUV position v: for instance in Figure 3b the two metrics $\overline{\Delta H_0}(v)$ and $\Delta H_{0,\max}(v)$ evaluated for $v = 2$ are reported at the bottom of the panel. By expanding the analysis across all other possible positions of the LUV, $\left(N_s^2 - 1\right)$ values of $\overline{\Delta H_0}(v)$ and $\Delta H_{0,\max}(v)$ are obtained, corresponding to each possible LUV location in the network. In the example shown in Figure 3, these metrics are displayed in the panel Figure 3c for each position of the LUV. Therefore, the values reported at a given junction in Figure 3c represent the cumulative network response associated with the installation of the LUV at that specific junction.

Finally, *network-focused* metrics provide a single value for the entire network by aggregating the *LUS-focused* results over all possible LUV locations. Specifically, we evaluated the mean and maximum values attained by $\overline{\Delta H_0}(v)$ and $\Delta H_{0,\max}(v)$ as v (the position of the LUV) varies. Panel *d* in Figure 3 illustrates these aggregated measures for the network in panel *a*.

In summary, the analysis produces three complementary sets of metrics: $\Delta H_0(v,n)$ at the junction level, $\overline{\Delta H_0}(v)$ and $\Delta H_{0,\max}(v)$ at the LUS level, and their average and maximum values at the network level. Together, they condense a large number of hydraulic simulations into a compact description of transient behavior, forming the basis for the subsequent exploration of links between hydraulic performance and WDN topology. To test the robustness of these findings against uncertainties in the network characteristics, we performed a sensitivity analysis in which key parameters were perturbed by ±10% across different scenarios. The resulting variations in $\overline{\Delta H_0}$, $\Delta H_{0,\max}$, and their spatial statistics confirmed that the proposed metrics are only moderately sensitive to

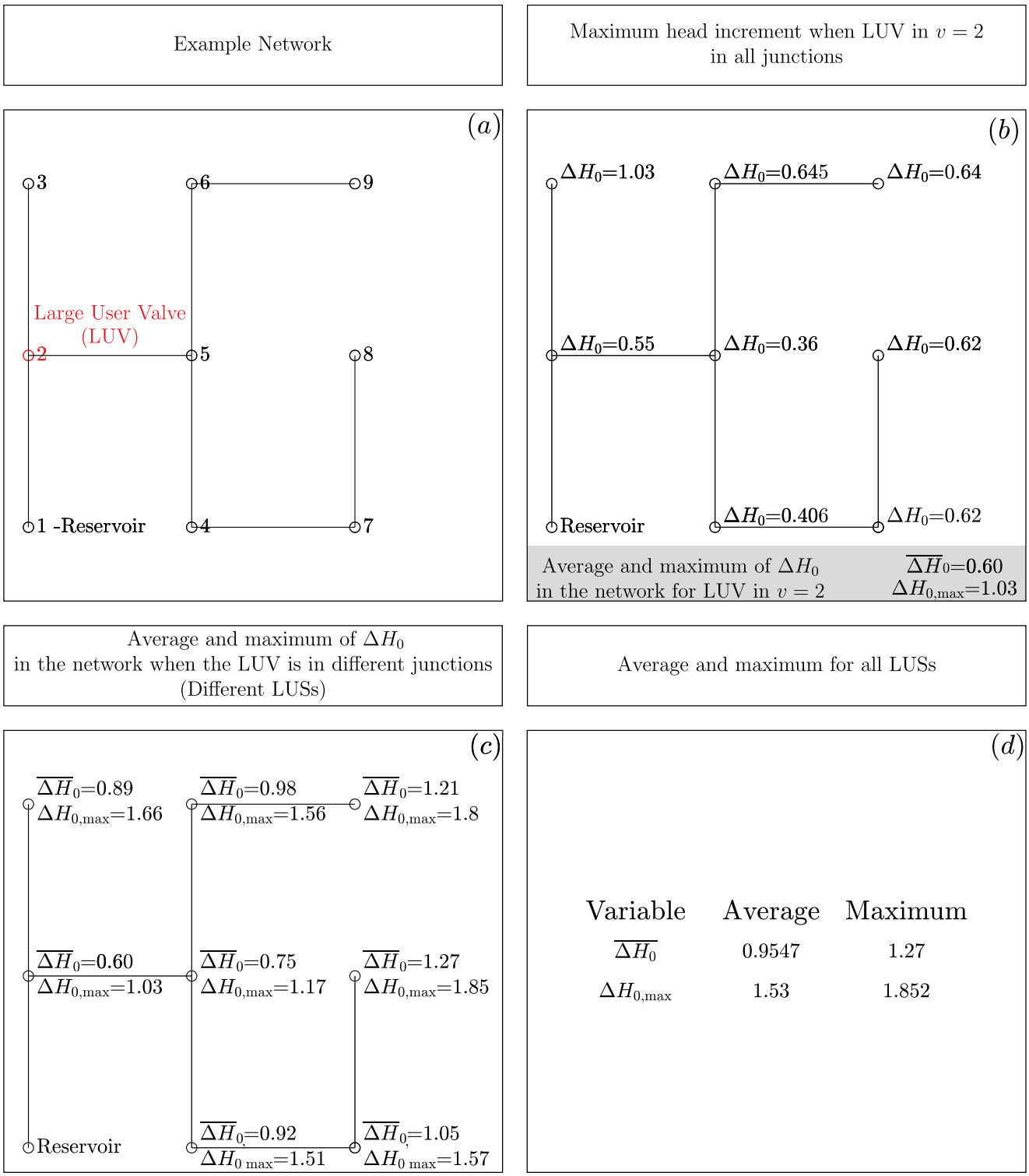

Figure 3. Example of the hydraulic metrics and their spatial/temporal aggregation procedure. (a) Layout of the example network ($N_s = 3, N = 9$) with the large user valve (LUV) at junction $v = 2$. (b) Junction-focused hydraulic metric $\Delta H_0(v,n)$, defined as the maximum (over time) head increment normalized by the steady-state head at each junction n due to the LUV closure. (c) LUS-focused hydraulic metrics $\overline{\Delta H_0}(v)$ (mean of ΔH_0 over all n) and $\Delta H_{0,\max}(v)$ (maximum of ΔH_0 over all n) for different LUV locations v. (d) Network-focused hydraulic metrics: mean and maximum values of $\overline{\Delta H_0}(v)$ and $\Delta H_{0,\max}(v)$ across all possible LUV locations. The interested reader can find in Supporting Information S1 the detailed, step-by-step procedure adopted to obtain the results presented here.

parameter uncertainties. Full details of this analysis, including quantitative ranges and supporting figures and tables, are reported in Supporting Information S1.

2.4. Topological Metrics

Although WDNs are not structurally as complex as social or biological networks, their topology and geometry can be characterized using tools from CNT (e.g., see the review by Yu et al. (2024)). In this framework, a network is described as a set of nodes (here, junctions) connected by links (here, pipes), and a variety of metrics can be computed to quantify different aspects of the network structure. These topological metrics are introduced to explore possible correlations with the hydraulic metrics defined in the previous section.

The connectivity of a WDN can be described by its weighted adjacency matrix $\mathbf{W}$, an $N \times N$ matrix where $W_{ij} > 0$ if a pipe connects nodes i and j, and $W_{ij} = 0$ otherwise. The pipe-specific value of $W_{ij} = w_p$ accounts for geometric or hydraulic properties of the pipe between nodes i and j. The choice of weights w_p and their relation to the pipe properties is discussed in the following sections.

The topological metrics are selected to represent structural features that are expected to influence both the magnitude and spatial distribution of maximum head variations within the network. Formal definitions of all the topological metrics adopted in this study are reported in Supporting Information S1. In the following, and consistent with the approach described in Section 2.3, we introduce these metrics at progressively larger levels of spatial aggregation.

Junction-focused metrics quantify local properties expected to influence head variations at individual junctions. These include the node degree (η_n), counting the number of pipes connected to the junction, and betweenness centrality (BC_n) (Freeman, 1977), measuring how nodes act as bridges or bottlenecks in network flows (Fellini et al., 2020). BC_n is based on the concept of shortest paths (e.g., Abraham et al., 2010): in a connected graph, there is at least one path connecting any pair of nodes that minimizes the number of links traversed. The betweenness centrality of a node then measures the fraction of these shortest paths that pass through it.

LUS-focused metrics describe the structural context of the LUV within the network. Relevant metrics include the degree (η_v) and betweenness centrality (BC_v) of the LUV node, as well as the shortest path between the reservoir and the LUV location (λ_{r-v}), providing a synthesized topological description of LUV position within the network.

Network-focused metrics characterize the network's overall (i) size, (ii) structure, (iii) interconnectivity, and (iv) efficiency of transport across it. Size metrics include the total number of links/pipes ($\mathcal{P}$) and the network diameter (*Dia*), defined as the shortest path between the two most distant nodes in the network. Structural metrics include Single-Degree Nodes (*DE*) and Meshness (*Mesh*). The *DE* metric counts the number of nodes in the network with a degree equal to one, meaning they are connected to only one neighbor. On the other hand, Meshness (Buhl et al., 2006) indicates whether the network exhibits a structure closer to a tree network (*Mesh* equal to 0) or a gridded network (*Mesh* equal to 0.5) (Martínez, 2010; Yazdani & Jeffrey, 2012). Interconnectivity metrics include the average degree (*AvgD*) of the network nodes, network density (*Den*), computed as the ratio between the actual number of links and the maximum possible number of links among the network nodes (M. Newman, 2018), and the algebraic connectivity (*AlgC*) that assesses the network's ability to maintain structural integrity when specific components are removed. Flow optimization metrics assess how efficiently the network transfers flow or information. These include the Sum of Betweenness Centrality (ΣBC), indicating the overall ability of nodes in facilitating flow through the network; the Average Shortest Path (L), representing the mean number of links connecting each node pair via the shortest path; and Network Efficiency (E) (Latora & Marchiori, 2001), measuring the average proximity between nodes using the harmonic mean of shortest paths. While L and E may seem similar, L is strongly influenced by nodes that are very distant from each other (shortest path is even ∞ for unconnected node pairs), whereas E emphasizes the overall efficiency of information or flow transfer, effectively discounting extremely distant or disconnected node pairs.

2.5. Topology-Based Model for Predicting Hydraulic Metrics

To assess the predictability of transient hydraulic behavior from topological metrics, we use the following multiplicative model

$$K = \prod_{\tau=1}^{N_T} T_\tau^{\alpha_\tau}, \tag{8}$$

where K is the hydraulic metric of interest (Section 2.3), T_τ is the τth topological metric (Section 2.4) used as a predictor, α_τ is its associated exponent, and N_T is the number of predictors. The model is fitted separately for each K. Taking logarithms yields the linear form

$$\log K = \sum_{\tau=1}^{N_T} \alpha_\tau \log T_\tau, \tag{9}$$

with coefficients α_τ estimated via standard least-squares minimization (Montgomery et al., 2021). As is customary, the goodness of fit of the resulting model is assessed using the coefficient of determination R^2, which expresses the proportion of variability explained (Montgomery et al., 2021).

The suitability of topological predictors for the hydraulic metric is assessed using stepwise selection. First, each predictor T_τ is evaluated individually ($N_T = 1$) and the one predicting K with the highest R^2 is selected as the first (best) predictor. Then, predictors are progressively added to the model in order to maximize R^2 at each addition, until no significant gain is obtained. This yields an ordered list of top predictors and the corresponding sequence of R^2 values, as will be discussed in Section 4.

3. Synthetic Water Distribution Networks

3.1. Generation of the WDNs

The correlations between the hydraulic and topological metrics presented in the previous sections were explored using a wide set of synthetic pipe networks, as commonly done in the literature (Marsili et al., 2023; Momeni et al., 2023; Torres et al., 2017). Using synthetic networks allows us to systematically control both the topology and the hydraulic properties of the system, generating a wide variety of scenarios with diverse hydraulic and topological characteristics. The shape of the synthetic network (regular grid) was chosen to be realistic, and representative of urban water distribution systems laying on a flat ground (Di Nardo et al., 2016; Santonastaso et al., 2020; Spizzo et al., 2023). This approach enables exploration of a broad range of hydraulic and topological metrics, which is essential for identifying correlations that are generalizable across different systems. Additionally, this approach allows us to apply a consistent set of rules for assigning hydraulic and network properties (e.g., pipe lengths and diameters) across all generated networks.

The synthetic WDNs were generated by varying the size and connectivity of the reference lattice described in Section 2.1, following the approach proposed by Torres et al. (2017). Specifically, square grids with N_s (junctions on edges) ranging from 3 to 10 were created (yielding networks with up to 100 junctions), with all elevations set to zero. Connections between junctions were then established based on a nodal connectivity probability, P_c, which defines the likelihood that two neighboring junctions are connected. We considered 6 values of P_c in the range $[0.2 - 0.7]$. Networks with $P_c = 1$ are fully connected grids, while lower values of P_c produce sparse, tree-like configurations. In details, for each junction, the list of potential connections with neighbors was compiled, including the nearest junctions located in the same row or column. For each potential connection, a random number in the interval [0, 1] was generated and compared to P_c. If the random number was lower than P_c, the connection was established, otherwise it was omitted (see the step-by-step procedure to build synthetic networks in Supporting Information S1).

P_c serves as an important indicator of overall network structure, influencing connectivity and redundancy. Therefore, in this study, P_c was a key parameter to build the network topology. We also included P_c in the set of topological metrics used to characterize the networks, because it can be easily calculated from existing networks (see the step-by-step procedure to calculate P_c in Supporting Information S1).

For each generated network, the connectivity test based on the second smallest eigenvalue of the network Laplacian matrix (M. Newman, 2018) was performed to ensure that no part of the network was isolated; network failing this test were discarded, and the generation process repeated. For each $\{N_s, P_c\}$ pair, three random networks

Table 1
Values (or Range of Values) of the Parameters That Were Used to Build the Synthetic Water Distribution Networks Considered in This Study

Parameter	Symbol	Unit	Value (or range of values)
Number of junction in each side of the lattice	N_s	(1)	3, 4, 5, 6, 7, 8, 9, 10
Probabilities of nodal connectivity	P_c	(1)	0.2, 0.3, 0.4, 0.5, 0.6, 0.7
Length of pipes in homogeneous networks	L_{HN}	(m)	30
Diameter of pipes in homogeneous networks	D_{HN}	(mm)	200
Celerity of the pressure wave	a_p	(m/s)	1,404, 1,340, 1,234
Coefficient for orifice flow	C_v	(1)	0.61
Size of the orifice at the LUV	A_v	(m^2)	$1 \cdot 10^{-3}$
Head of reservoir	h_r	(m)	50

were generated to enlarge the pool of configurations considered. We obtained networks with a number of connections (pipes) varying between 9 and 180.

The final step consisted of assigning lengths and diameters to the established pipes, following two distinct approaches. In the first approach, all pipes in a network were assigned the same length L_{HN} and diameter D_{HN} (i.e., $L_p = L_{HN}$ and $D_p = D_{HN}$ for $p = 1 \ldots P$). The corresponding networks are refereed to as *Networks with homogeneous pipes* (HNs). The hydraulic parameters of the synthetic networks (see Table 1) were chosen to produce realistic networks, representative of a small-medium urban water distribution systems. The obtained networks were in fact made up of 9–100 junctions and spanned an area between 8,100 and 90,000 square meters. The total flow rate delivered to the network was between 10 and 200 l/s, making the network considered as representative of quite densely populated area. Finally, the demand at the main junction was of the order of 10 l/s, representative of a medium/large commercial/industrial user.

In the second approach, intra-network variability in pipe lengths and diameters was introduced, obtaining *Networks with non-homogeneous pipes* (NHNs). For each HN, three types of variations were created: (i) a network with each pipe length randomly selected from $[0.5, 1, 2]L_{HN}$; (ii) a network with each pipe diameter randomly selected from $[0.5, 1, 2]D_{HN}$; (iii) a network with both lengths and diameters randomly selected as shown in steps (i) and (ii). This process was repeated three times for every HN, resulting in nine NHNs derived from each HN. The networks generated with this approach could be non-realistic: the spatial allocation of pipe diameters were in fact not tied to actual demand patterns or service constraints. This deliberate decoupling was adopted to test the validity of our method, which regresses hydraulic metrics on topology metrics, under extreme but controlled conditions. In this way, we aimed to isolate topology effects and assess the robustness of the regression beyond case-specific details. Altogether, 144 network topologies were generated, resulting in 144 HNs and 1,296 NHNs. In total, 4,488,480 time series of piezometric head were obtained from simulations and analyzed.

3.2. Hydraulic and Topological Characteristics of the Generated WDNs

After the generation procedure described above, the synthetic WDNs are analyzed to determine their key hydraulic properties and topological characteristics. This step serves both to verify the diversity of the generated networks and to identify the order of magnitude and the range of variation of the predictors used in the subsequent analysis.

We first analyze the main hydraulic characteristics of the synthetic WDNs under steady-state conditions, before closure of the LUV. Figures 4a–4c shows histograms for: (*a*) pressure-driven outflow at junctions; (*b*) flow rate in the pipes; and (*c*) head at the junctions. Results are distinguished between homogeneous networks (HNs, blue) and non-homogeneous networks (NHNs, orange). Histograms are normalized so that their area equals unity, as in a probability density function.

The outflow distribution (Figure 4a) reveals significant variability with two distinct peaks. The left peak, around 1.5 l/s, corresponds to the small pressure-driven outflow applied uniformly to all network junctions and is similar for both HNs and NHNs.The right peak, occurring at a much lower frequency ($\sim 10^{-3}$ vs. $\sim 10^{-1}$), represents

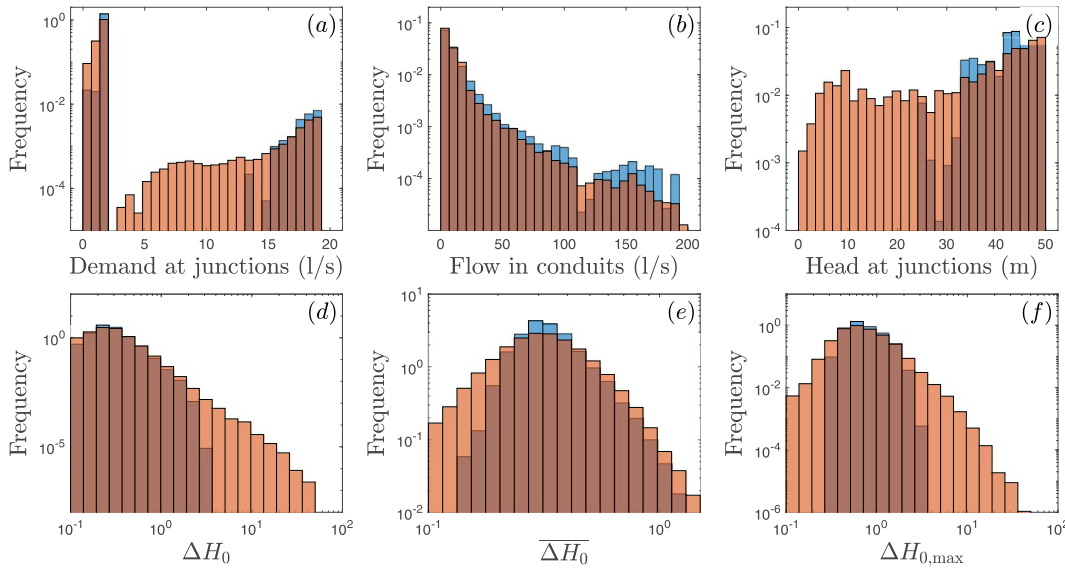

Figure 4. Histograms of some relevant hydraulic characteristics (steady state and transient flow conditions) of the synthetic water distribution networks (WDNs) that were considered in this study (see the label of the horizontal axis). Do note that some axes are in a logarithmic scale. Orange refers to WDN with non-homogeneous pipes, blue refers to WDN with homogeneous pipes. The height of bars was normalized so that the area of the histogram is equal to unity (as in a pdf distribution).

junctions where the LUV is installed. In this case, HNs exhibit a relatively narrow outflow range (15–20 l/s), whereas NHNs display a broader range (4–20 l/s). This increased variability in NHNs arises from zones with low hydraulic conductivity, caused by longer, smaller-diameter pipes that can restrict the outflow from the LUV.

Figure 4b shows the flow-rate distribution in the pipes. Most pipes convey flows below 10 l/s, with only a few reaching around 100 l/s. Differences between HNs and NHNs appear mainly in the right tail, where high flow-rates are less frequent in NHNs, again due to low-conductivity pipes limiting the flow in certain areas of the networks.

The head distribution at junctions (Figure 4c) also differs between HNs and NHNs. In HNs, head values remain above 25 m, resulting in a histogram with two distinct peaks. The left peak, around 25 m, corresponds to junctions near the LUV, where higher outflow reduces the head. In contrast, NHNs exhibit a wider range of head values: while many junctions have head above 20–25 m, some can drop as low as 2 m. These low-head junctions occur when the LUV is connected to the network through pipes with low hydraulic conductivity.

We then examine the hydraulic response under transient conditions, accounting for the LUV closure. Figures 4d and 4e report histograms for the key hydraulic metrics introduced in Section 2.3: ΔH_0, $\overline{\Delta H_0}$, and $\Delta H_{0,\max}$. We also analyzed the spatially averaged and maximum values of $\overline{\Delta H_0}$ and $\Delta H_{0,\max}$, with results provided in Supporting Information S1. Although both HNs and NHNs show single-peaked distributions at approximately the same values, NHNs consistently exhibit: (i) broader distributions, indicating higher variability in transient response, and (ii) fatter tails, reflecting a greater occurrence of extreme values.

These differences stem from the underlying network characteristics. In NHNs, some junctions have low steady-state head (Figure 4c), which increases the relative pressure surge ratios (Equation 5), producing larger water hammer metrics and a fatter right tail in the distributions. Additionally, NHNs may contain partially isolated zones—caused by long, small-diameter pipes—where pressure surges are minimal, resulting in a fatter left tail in the distributions.

As with the hydraulic characteristics of the synthetic WDNs, it is also interesting to examine the distributions of the networks' topological properties. These distributions are reported in Figure S6 in Supporting Information S1 and are distinguished between homogeneous (HNs) and NHNs. A detailed discussion of the order of magnitude, variability and distributions shown by the different topological metrics is provided in Supporting Information S1.

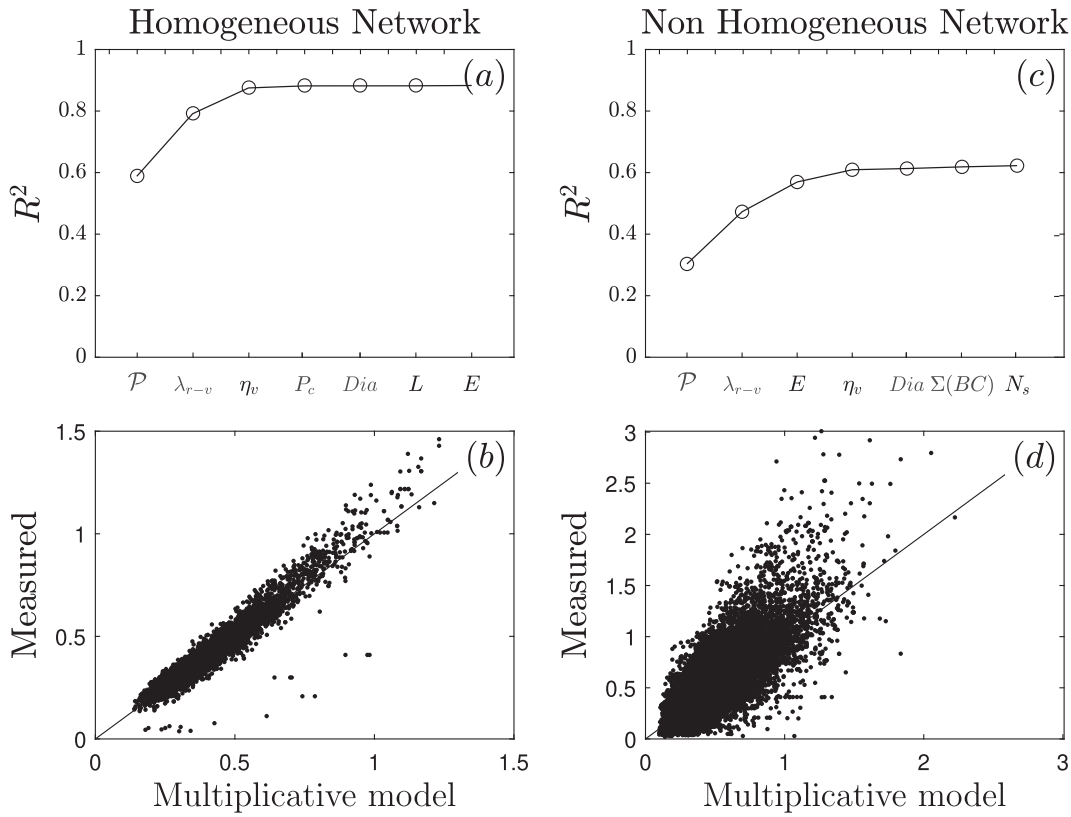

Figure 5. Applications of the model (8) for estimating $\overline{\Delta H}_0$ in homogeneous networks (left panels) and non-homogeneous networks (right panels). Panels (a) and (c) illustrate how the R^2 value decreases progressively as the number of predictors in the model increases. Panels (b) and (d) depict the performance of the full model (incorporating all predictors) in the measured versus estimated plane.

4. Results

4.1. Regression Model Performance Across Hydraulic Metrics

We evaluated how network topology can explain average and maximum head increments in synthetic WDNs under transient flow conditions. To this end, we applied the multiplicative regression model (Section 2.5) to the set of networks generated according to Section 3. For each hydraulic metric, the topological predictors were tested and ranked according to their incremental contribution to maximizing R^2, as detailed in Section 2.5.

All topological metrics are computed as weighted quantities, where link weights account for pipe geometry and hydraulic properties. In HNs, where all pipes have identical length and diameter, the link weights are equal. For such networks, the regression model (9) yields excellent predictive performance. As an illustrative example of the stepwise application of the regression model described in Text S9 in Supporting Information S1, Figure 5 shows how predictors are progressively added to maximize R^2 for a single hydraulic metric. For $\overline{\Delta H}_0$ (average head increment in the network following closure of a specific LUV), the best single predictor is $\mathcal{P}$ (total number of links), giving $R^2 = 0.59$ (Figure 5a). Adding λ_{r-v} (shortest path between reservoir and LUV) increases R^2 to 0.79, and including 3–4 predictors further improves R^2 to about 0.90, beyond which no substantial gain is observed. The full model (all topological metrics) reproduces the hydraulic metric values with high accuracy (Figure 5b).

For NHNs, variability in pipe lengths and diameters requires assigning link weights consistent with each pipe's properties to achieve good predictive performance. Several weighting formulations were evaluated, including L_p/D_p^2, L_p/D_p, $L_p \cdot D_p$, $L_p \cdot D_p^{1/2}$, a_p/L_p, $(a_p/L_p)^2$, and $(a_p/L_p)^{1/2}$. The best performing weight, yielding the highest R^2 values, was $w_p = L_p/D_p^2$, which reflects the time required for the pressure surge to transit along the pipe. Figures 5c and 5d provides a numerical example showing the stepwise addition of predictors for $\overline{\Delta H}_0$ in

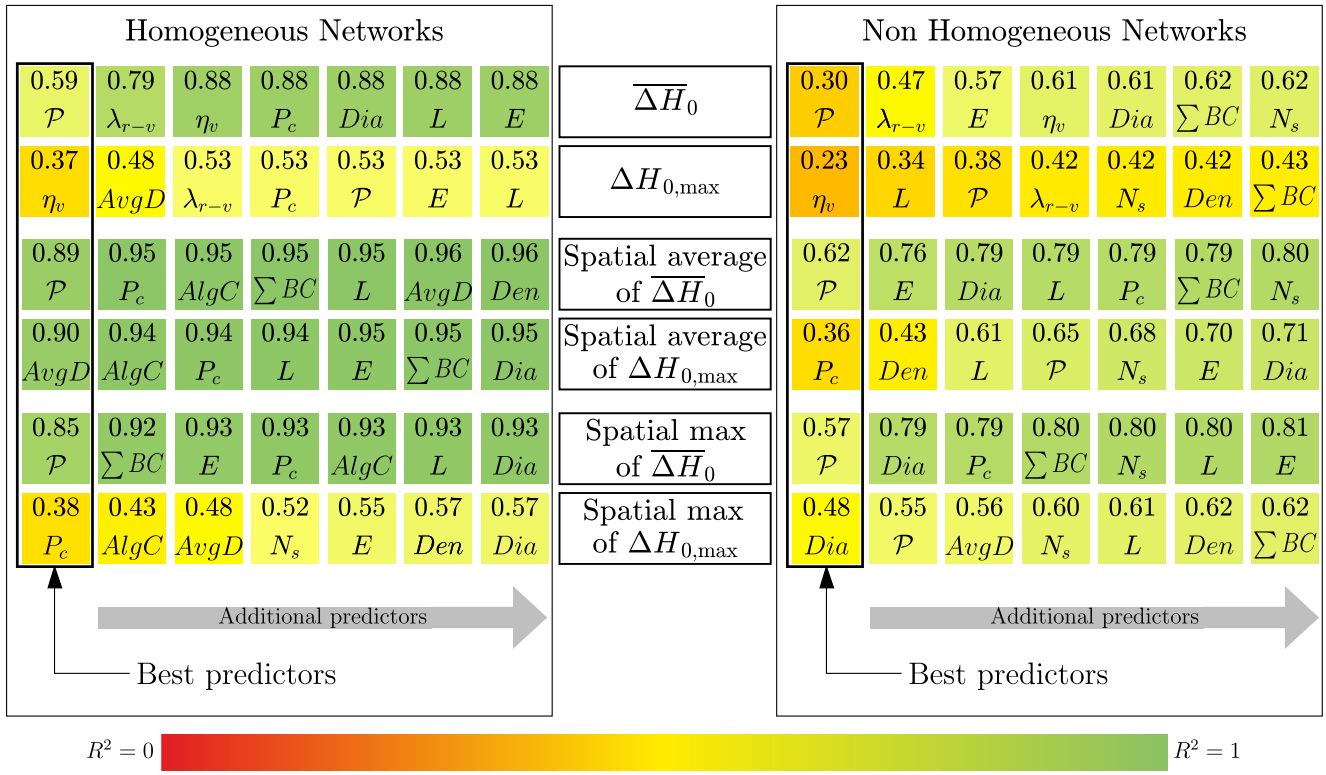

Figure 6. Performance of predictors (topological metrics) in explaining the variability of hydraulic metrics. Each line reports: (i) the hydraulic metric considered (white box); (ii) the first 7 predictors selected by the regression model and the cumulative R^2 achieved (reported in the colored boxes). Boxes on the left, correspond to homogeneous networks, while those on the right correspond to non-homogeneous networks. Predictors are ordered from left to right, with the most influential (best) predictor in the leftmost column, highlighted with a black border. Colors are as follows: red $R^2 = 0$; yellow $R^2 = 0.50$, green $R^2 = 1.00$. Shades between these colors refers to intermediate values of R^2 (see also the color-bar).

NHNs. Using this weighting, R^2 increased progressively to about 0.65 with 4–5 predictors (panel c), and the full model reproduced the hydraulic metric values with good agreement between predicted and simulated results (panel d).

Building on the illustrative example presented in Figure 5 for a single hydraulic metric $(\overline{\Delta H_0})$, Figure 6 summarizes the results of the stepwise regression model across all *LUS-focused* and *network-focused* hydraulic metrics defined in Section 2.3. *Junction-focused* metrics could not be reliably predicted and are therefore not reported. In Figure 6, each row shows how R^2 increases as topological predictors are progressively added, providing a comprehensive view of model performance for each metric.

For HNs (left panel of Figure 6), the model provides excellent fits for 4 out of 6 hydraulic metrics: $\overline{\Delta H_0}$, the spatial averages of $\overline{\Delta H_0}$ and $\Delta H_{0,\max}$, and the spatial maximum of $\overline{\Delta H_0}$. The highest performance is achieved for the spatial average of ΔH_0, where R^2 reaches a maximum value of 0.96 using only 6 predictors (see the third row of the left panel in Figure 6). The remaining two metrics, $\Delta H_{0,\max}$ and its spatial maximum, are less well predicted, with a minimum R^2 of 0.53.

For NHNs (right side of Figure 6), the model (considering the weights $w_p = L_p/D_p^2$) performs well for 3 out of 6 hydraulic metrics: the spatial averages of $\overline{\Delta H_0}$ and $\Delta H_{0,\max}$, and the spatial maximum of $\overline{\Delta H_0}$. For these metrics, R^2 values are above 0.62, reaching up to 0.81, again with fewer than 7 predictors. However, for the remaining 3 metrics ($\overline{\Delta H_0}$, $\Delta H_{0,\max}$, and its spatial maximum), R^2 values are lower, with a minimum of 0.43.

In general, for both HNs and NHNs, the ability of topology in explaining hydraulic variability diminishes when moving from spatially averaged metrics (e.g., the spatial average of $\overline{\Delta H_0}$) to more localized metrics (e.g., the spatial maximum of $\Delta H_{0,\max}$). This suggests that local effects of hydraulic transients depend on local network

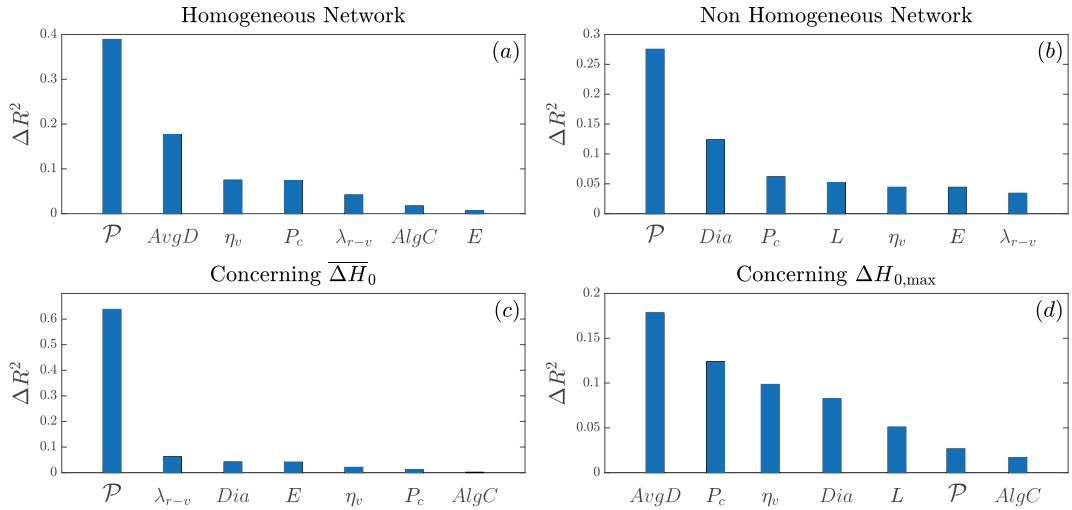

Figure 7. Relevance charts of different predictors. The values reported in panel (a, (b)) were evaluated considering homogeneous networks (non-homogeneous networks) only. The values reported in panel (c) refer to the hydraulic metric $\overline{\Delta H}_0$, its spatial average, and its spatial maximum. The values reported in panel (d) refer to the hydraulic metric $\Delta H_{0,\max}$, its spatial average, and its spatial maximum.

characteristics (both topological and geometric) that are not fully captured by the topological metrics considered in this study. Interestingly, $\overline{\Delta H}_0$ was well predicted by topology in HNs, with R^2 reaching 0.88. For NHNs, the predictive power decreased to 0.62, showing that local effects become more important and that the considered topological metrics cannot fully capture certain transient behaviors.

4.2. Key Topological Predictors Across Hydraulic Metrics

To go beyond simply assessing the predictive ability of topological metrics for water hammer effects, we aimed to identify which metrics have the greatest impact. We quantified the contribution of each topological metric using $\Delta R^2_K(T_\tau)$, which represents the increment in R^2 for the Kth hydraulic metric when the predictor T_τ is added to the regression model (8). For example, Figure 5a shows that adding λ_{r-v} to the model for $\overline{\Delta H}_0$ raises R^2 from 0.59 to 0.79, giving $\Delta R^2_{\overline{\Delta H}0}(\lambda_{r-v}) = 0.20$. The most important predictor (the first one selected for the regression model) typically shows the largest $\Delta R^2_K(T_\tau)$ (e.g., $\Delta R^2_{\overline{\Delta H}_0}(\mathcal{P}) = 0.59$).

To summarize the relevance of each topological metric across all hydraulic metrics, we define its global relevance as $\Delta R^2(T_\tau)$, which is the average of $\Delta R^2_K(T_\tau)$ over all K. A higher $\Delta R^2(T_\tau)$ indicates that the predictor frequently improves model performance across multiple hydraulic metrics.

Panels *a* and *b* in Figure 7 display the global relevance (ΔR^2) of the topological metrics considered in this study, separately for HNs (Panel *a*) and NHNs (Panel *b*). For both HNs and NHNs, the most significant predictor was $\mathcal{P}$, the number of links in the network, with $\Delta R^2(\mathcal{P}) > 0.4$ for HNs and $\Delta R^2(\mathcal{P}) > 0.25$ for NHNs. Other key predictors contributing significantly to R^2 in both cases included: (i) the degree of the node where the LUV is installed (η_v), (ii) the connection probability (P_c), and (iii) the distance between the reservoir and the LUV (λ_{r-v}). For HNs, another relevant predictor was the average degree (*AvgD*), while for NHNs, additional important predictors were: (i) network diameter (*Dia*), (ii) the average shortest path (*L*), and (iii) network efficiency (*E*).

We also assessed in Panels *c* and *d* the global relevance (ΔR^2) of the topological metrics in explaining specific groups of hydraulic metrics: those associated with $\overline{\Delta H}_0$ (i.e., $\overline{\Delta H}_0$, its spatial average, and its spatial maximum), and those associated with $\Delta H_{0,\max}$ (i.e., $\Delta H_{0,\max}$, its spatial average, and its spatial maximum). In this case, both HNs and NHNs were considered together. Hydraulic metrics related to $\overline{\Delta H}_0$ (Figure 7c) showed a strong dependence on $\mathcal{P}$, with $\Delta R^2(\mathcal{P}) > 0.6$. Other significant predictors included λ_{r-v}, *Dia*, *E*, η_v, and P_c. Notably, the second most influential predictor, λ_{r-v}, had a relevance approximately one-tenth that of $\mathcal{P}$ $(\Delta R^2(\lambda_{r-v}) \sim 0.07)$. In contrast, the relationship between topological metrics and the hydraulic metrics related to $\Delta H_{0,\max}$ is less

straightforward. Several predictors, such as $AvgD$, P_c, η_v, and Dia, showed lower relevance values around 0.1. Additionally, metrics such as L, $\mathcal{P}$, $AlgC$, Den, λ_{r-v}, and E displayed relevance values in the range of approximately 0.05.

5. Discussion

In the previous section, we demonstrated that topological metrics can significantly explain the transient response of a network subjected to the shutting of the outflow to a large user. Now, it is essential to discuss the characteristics of the different predictors and, where possible, derive physical insights.

We specifically focus on the topological predictors that performed best in Figure 6 and were globally relevant across all regression models (i.e., those that ranked among the top predictors in the charts in Figure 7).

It is crucial to note that a clear physical interpretation of the role of topological metrics is possible only when they serve as the best predictors. Therefore, we evaluated model (9) using only the best predictor (highlighted in Figure 6) for each hydraulic metric. We then computed the sign of the corresponding coefficient, α_{τ^*}, to determine whether the best predictor contributes to increasing or decreasing the corresponding hydraulic metric.

Number of Pipes, $\mathcal{P}$. The number of pipes, $\mathcal{P}$, was identified as the most influential metric. It exhibited the highest relevance $\left(\Delta R^2\right)$ in Figure 7 and was the best predictor in the regression models for many hydraulic metrics (6 out of 12, as shown in Figure 6). When $\mathcal{P}$ was the best predictor, it was always associated with a negative exponent in the model (9), indicating that larger values of $\mathcal{P}$ correspond to less severe flow transients.

The relevance of $\mathcal{P}$ can be explained physically: as the number of pipes increases, more pathways are available for pressure waves to propagate. This increases the likelihood that the initial pressure surge splits into multiple pipes, reducing its magnitude. Furthermore, an increased number of pipes enhances the network's water delivery capacity, resulting in lower pipe velocities. According to Joukovski's law (Chaudhry, 2014; Joukowksy, 1900), this in turn reduces head variations during transients.

Network Diameter, Dia. Another important topological metric is the network diameter, Dia, which is defined as the maximum shortest path between any pair of junctions. As shown in Figure 6 (last line, right side), Dia was the best predictor for the spatial maximum of $\Delta H_{0,\max}$ in NHNs. The relationship observed was that larger diameters resulted in less severe flow transients.

The effect of Dia can be understood by recognizing that in networks with smaller diameters, pressure waves are confined to a smaller system. A small diameter results in quick reflection of pressure waves, preventing them from propagating long distances and splitting. This interaction between positive wavefronts with significant amplitude tends to generate high values of $\Delta H_{0,\max}$. In contrast, in a network with a larger diameter, pressure waves can propagate over longer distances, splitting multiple times before reaching the furthest nodes, where they are eventually reflected.

Degree of the LUV node, η_v. The results in Figure 6 (second line) show that the degree of the LUV junction, η_v, is the best predictor for the maximum head increment $(\Delta H_{0,\max})$ observed in the network after the LUV closure. The larger the value of η_v, the less severe the flow transients. This relationship holds true for both HNs and NHNs. We note that, unlike the cases discussed above, the relationship between η_v and $\Delta H_{0,\max}$ is a very local one, providing information about the maximum head increment observed in network after the closure of a specific LUV (v).

As the number of pipes departing from the LUV (node $n = v$) increases, pressure waves have more pathways to propagate, enhancing the likelihood that the original pressure surge splits into multiple pipes and reduces its initial magnitude. Additionally, increasing the number of pipes supplying the large user reduces water velocity in the pipes, and according to Joukovski's law, this leads to smaller head variations during transients.

Average degree of network nodes, $AvgD$. As shown in the fourth row of Figure 6, $AvgD$ was the best predictor for the spatial average of $\Delta H_{0,\max}$ in homogeneous hydraulic networks (HNs). In other words, the average number of pipes per junction across the entire network serves as an excellent predictor of the maximum head increments that occur, on average, across all possible LUSs. Specifically, a higher $AvgD$ is associated with less severe flow transients.

Consistently, Panel *d* of Figure 7 highlights that *AvgD* is the most important predictor (i.e., the one with the highest relevance ΔR^2) when considering all metrics related to the maximum head increment ($\Delta H_{0,\max}$).

The role of *AvgD* is closely linked to the explanation provided for η_v. As the number of pipes connected to each junction increases, pressure waves have more pathways for propagation, enhancing the likelihood that the original pressure surge will split into multiple pipes, thereby reducing its initial magnitude.

However, unlike η_v, which is the best predictor of the single highest head increment observed in the network, *AvgD* provides an averaged measure of all peak values recorded following the LUV closure across all possible LUSs. This distinction is meaningful, as *AvgD* reflects the connectivity of the entire network, considering the number of pipes branching from every junction, whereas η_v is a local metric that pertains specifically to the node where the LUV is located.

Probability of connection, P_c. Another key metric reflecting the network's interconnectivity is P_c. When P_c was the best predictor, higher values were associated with less severe flow transients. Specifically, P_c emerged as the best predictor for the maximum head increment in HNs considering all possible LUV positions. It was also the best predictor for the average of the maximum head increments across the network for different LUSs.

Similar to *AvgD*, the relevance of P_c is linked to the number of pipes connected to each junction. As this number increases, pressure waves have more pathways for propagation, increasing the likelihood of the original pressure surge splitting into multiple pipes and thereby reducing its initial magnitude. Given this mechanism, it is unsurprising that P_c, like *AvgD*, plays a crucial role in predicting maximum head increments in the network.

Other topological metrics played a role in explaining transient responses in hydraulic networks. The interested reader can find in Supporting Information S1 a discussion concerning those topological metrics.

6. Concluding Remarks

Flow transient dynamics is a complex process that involves both linear and nonlinear mechanisms of wave propagation, reflection, dissipation, and interference. When pressure surges propagate through a pipe network, additional mechanisms come into play, such as partial wave reflections at junctions, and outflows to end users. Wave interferences also become significantly more frequent compared to the single-pipe case (e.g., a water main).

To investigate the role of network topology, we numerically simulated the water hammer phenomenon following closure of the valve controlling the outflow of a large user. A large set of networks with varying topological and geometric characteristics was considered. Our main findings are twofold: (i) connectivity structure plays a crucial role in shaping pressure surges within hydraulic networks, and (ii) when appropriately combined with pipe geometric properties (length and diameter), certain topological metrics derived from CNT can, combined in multivariate multiplicative regression models, provide accurate estimates of water hammer effects (e.g., four to five carefully selected topological metrics can account for up to 90% of the variability observed in specific hydraulic metrics). Importantly, the most informative topological metrics admit a clear hydraulic interpretation. Consequently, multiplicative multivariate models are not merely interpolation artifacts but offer meaningful physical insights into the transient response of networks.

However, the key point of our analysis is not the specific form of the network models, the actual values of the coefficients, or the specific metric used to measure the adherence between model and observations, but rather to demonstrate the key role of topology in the water hammer phenomenon. Topological metrics alone can explain up to 96% of the variance (as measured by the R^2 coefficient) of hydraulic metrics describing flow transients. This result provides new evidence of the role of topology, despite the fact that flow transients are dominated by nonlinear processes that could easily mask or rule out such effects. Indeed, in several classical dynamical systems the nonlinearities enforce a unique global attractor, making the final outcome independent of network structure. For example, in consensus dynamics (Olfati-Saber et al., 2007), Kuramoto synchronization at strong coupling (Acebrón et al., 2005; Strogatz, 2000), diffusion to equilibrium (Chung, 1997; Masuda et al., 2017), epidemic spreading without recovery (Pastor-Satorras & Vespignani, 2001; M. E. Newman, 2002), and evolutionary games with strict dominance (Nowak, 2006; Szabó & Fáth, 2007). Our findings therefore highlight a clear and quantifiable contribution of topology to transient behavior.

Our results have significant implications for the design, maintenance, and safety of WDNs. In fact, the possibility of estimating the unsteady response of networks solely from their topological features paves the way for rapid and systematic preliminary assessments of water hammer impacts, without the need for extensive and time-consuming simulations. A large number of cases (different topologies, multiple closure scenarios, and varying pipe properties) can thus be easily explored. Once the most critical and relevant cases have been identified in this way, they can then be investigated through detailed numerical simulations.

Finally, our study also suggests general best practices for managing WDNS. For instance, networks with larger diameters and greater number of pipes tend to experience less severe surges, whereas strategies such as districtualization, which reduce network size, can have unintended adverse effects on transient behavior. Likewise, parameters such as P_c and $AvgD$ are essential in attenuating flow transients; modifications that diminish their value may dangerously increase surge magnitudes. Overall, these insights can guide network operation without inadvertently compromising safety under unsteady conditions.

Conflict of Interest

The authors declare no conflicts of interest relevant to this study.

Data Availability Statement

At the link https://doi.org/10.5281/zenodo.17878272 is possible to download: (i) the dataset containing all the networks considered in this study; (ii) a MATLAB script for calculating the hydraulic metrics; (iii) a MATLAB script for calculating the topological metrics; (iv) a MATLAB script for implementing the regression analysis.

Acknowledgments
This work was carried out as part of the authors' institutional research activities and received no specific external funding. Open access publishing facilitated by Politecnico di Torino, as part of the Wiley - CRUI-CARE agreement.

References

Abraham, I., Fiat, A., Goldberg, A. V., & Werneck, R. F. (2010). Highway dimension, shortest paths, and provably efficient algorithms. In *Proceedings of the twenty-first annual ACM-SIAM symposium on discrete algorithms* (pp. 782–793).

Acebrón, J. A., Bonilla, L. L., Vicente, C. J. P., Ritort, F., & Spigler, R. (2005). The kuramoto model: A simple paradigm for synchronization phenomena. *Reviews of Modern Physics*, *77*(1), 137–185. https://doi.org/10.1103/revmodphys.77.137

Albert, R., & Barabási, A.-L. (2002). Statistical mechanics of complex networks. *Reviews of Modern Physics*, *74*(1), 47–97. https://doi.org/10.1103/revmodphys.74.47

Barthélemy, M. (2011). Spatial networks. *Physics Reports*, *499*(1–3), 1–101. https://doi.org/10.1016/j.physrep.2010.11.002

Boccaletti, S., Bianconi, G., Criado, R., del Genio, C., Gómez-Gardeñes, J., Romance, M., et al. (2014). The structure and dynamics of multilayer networks. *Physics Reports*, *544*(1), 1–122. https://doi.org/10.1016/j.physrep.2014.07.001

Boccaletti, S., Latora, V., Moreno, Y., Chavez, M., & Hwang, D.-U. (2006). Complex networks: Structure and dynamics. *Physics Reports*, *424*(4–5), 175–308. https://doi.org/10.1016/j.physrep.2005.10.009

Buhl, J., Gautrais, J., Reeves, N., Solé, R. V., Valverde, S., Kuntz, P., & Theraulaz, G. (2006). Topological patterns in street networks of self-organized urban settlements. *European Physical Journal B: Condensed Matter and Complex Systems*, *49*(4), 513–522. https://doi.org/10.1140/epjb/e2006-00085-1

Chaudhry, M. H. (2014). *Applied hydraulic transients* (Vol. 415). Springer.

Chung, F. R. K. (1997). *Spectral graph theory* (Vol. 92). American Mathematical Society.

Costa, L. D. F., Oliveira, O. N., Jr., Travieso, G., Rodrigues, F. A., Villas Boas, P. R., Antiqueira, L., et al. (2011). Analyzing and modeling real-world phenomena with complex networks: A survey of applications. *Advances in Physics*, *60*(3), 329–412. https://doi.org/10.1080/00018732.2011.572452

de Schaetzen, W., Walters, G., & Savic, D. (2000). Optimal sampling design for model calibration using shortest path, genetic and entropy algorithms. *Urban Water*, *2*(2), 141–152. https://doi.org/10.1016/s1462-0758(00)00052-2

Di Nardo, A., & Di Natale, M. (2011). A heuristic design support methodology based on graph theory for district metering of water supply networks. *Engineering Optimization*, *43*(2), 193–211. https://doi.org/10.1080/03052151003789858

Di Nardo, A., di natale, M., Giudicianni, C., Greco, R., & Santonastaso, G. (2016). Water supply network partitioning based on weighted spectral clustering. *Studies in Computational Intelligence*, *693*, 797–807. https://doi.org/10.1007/978-3-319-50901-3_63

Dunn, S., & Wilkinson, S. (2013). Identifying critical components in infrastructure networks using network topology. *Journal of Infrastructure Systems*, *19*(2), 157–165. https://doi.org/10.1061/(asce)is.1943-555x.0000120

Fellini, S., Salizzoni, P., & Ridolfi, L. (2020). Centrality metric for the vulnerability of urban networks to toxic releases. *Physical Review E*, *101*(3), 032312. https://doi.org/10.1103/physreve.101.032312

Fellini, S., Salizzoni, P., & Ridolfi, L. (2021). Vulnerability of cities to toxic airborne releases is written in their topology. *Scientific Reports*, *11*(1), 23029. https://doi.org/10.1038/s41598-021-02403-y

Freeman, L. (1977). A set of measures of centrality based on betweenness. *Sociometry*, *40*(1), 5–41. https://doi.org/10.2307/3033543

Giustolisi, O., Ciliberti, F. G., Berardi, L., & Laucelli, D. B. (2022). A novel approach to analyze the isolation valve system based on the complex network theory. *Water Resources Research*, *58*(4), e2021WR031304. https://doi.org/10.1029/2021wr031304

Giustolisi, O., & Ridolfi, L. (2014). A novel infrastructure modularity index for the segmentation of water distribution networks. *Water Resources Research*, *50*(10), 7648–7661. https://doi.org/10.1002/2014wr016067

Giustolisi, O., Ridolfi, L., & Simone, A. (2019). Tailoring centrality metrics for water distribution networks. *Water Resources Research*, *5*(3), 2348–2369. https://doi.org/10.1029/2018wr023966

Giustolisi, O., Simone, A., & Ridolfi, L. (2017). Network structure classification and features of water distribution systems. *Water Resources Research*, *53*(4), 3407–3423. https://doi.org/10.1002/2016wr020071

Huang, Y., Duan, H.-F., Zhao, M., Zhang, Q., Zhao, H., & Zhang, K. (2017). Transient influence zone based decomposition of water distribution networks for efficient transient analysis. *Water Resources Management*, *31*(6), 1915–1929. https://doi.org/10.1007/s11269-017-1621-x

Iacobello, G., Ridolfi, L., & Scarsoglio, S. (2021). A review on turbulent and vortical flow analyses via complex networks. *Physica A: Statistical Mechanics and its Applications*, *563*, 125476. https://doi.org/10.1016/j.physa.2020.125476

Joukowksy, N. (1900). Über den hydraulischen stoss in wasserleitungsröhren: Vorgelegt der akademie am 13. Mai 1898. In *Académie impériale des sciences*.

Khoa Bui, X., Marlim, S., & Kang, D. (2020). Water network partitioning into district metered areas: A state-of-the-art review. *Water*, *12*(4), 1002. https://doi.org/10.3390/w12041002

Latora, V., & Marchiori, M. (2001). Efficient behavior of small-world networks. *Physical Review Letters*, *87*(19), 198701. https://doi.org/10.1103/physrevlett.87.198701

Mala-Jetmarova, H., Barton, A., & Bagirov, A. (2015). A history of water distribution systems and their optimisation. *Water Science and Technology: Water Supply*, *15*(2), 224–235. https://doi.org/10.2166/ws.2014.115

Marsili, V., Alvisi, S., Maietta, F., Capponi, C., Meniconi, S., Brunone, B., & Franchini, M. (2023). Extending the application of connectivity metrics for characterizing the dynamic behavior of water distribution networks. *Water Resources Research*, *59*(8), e2023WR035031. https://doi.org/10.1029/2023wr035031

Martínez, J. (2010). Cost and reliability comparison between branched and looped water supply networks. *Journal of Hydroinformatics*, *12*(2), 150–160. https://doi.org/10.2166/hydro.2009.080

Masuda, N., Porter, M. A., & Lambiotte, R. (2017). Random walks and diffusion on networks. *Physics Reports*, *716–717*, 1–58. https://doi.org/10.1016/j.physrep.2017.07.007

May, J. (1994). Pressure dependent leakage. *World Water and Environmental Engineer*, *17*(8), 10.

Meng, F., Fu, G., Farmani, R., Sweetapple, C., & Butler, D. (2018). Topological attributes of network resilience: A study in water distribution systems. *Water Research*, *143*, 376–386. https://doi.org/10.1016/j.watres.2018.06.048

Meniconi, S., Brunone, B., & Frisinghelli, M. (2018). On the role of minor branches, energy dissipation, and small defects in the transient response of transmission mains. *Water*, *10*(2), 187. https://doi.org/10.3390/w10020187

Meniconi, S., Maietta, F., Alvisi, S., Capponi, C., Marsili, V., Franchini, M., & Brunone, B. (2022). Consumption change-induced transients in a water distribution network: Laboratory tests in a looped system. *Water Resources Research*, *58*(10), e2021WR031343. https://doi.org/10.1029/2021wr031343

Momeni, A., Chauhan, V., Bin Mahmoud, A., Piratla, K. R., & Safro, I. (2023). Generation of synthetic water distribution data using a multiscale generator-optimizer. *Journal of Pipeline Systems Engineering and Practice*, *14*(1), 04022074. https://doi.org/10.1061/JPSEA2.PSENG-1358

Montgomery, D. C., Peck, E. A., & Vining, G. G. (2021). *Introduction to linear regression analysis*. John Wiley & Sons.

Nault, J., Karney, B., & Jung, B. (2016). Algebraic water hammer: Global formulation for simulating transient pipe network hydraulics. In *World environmental and water resources congress 2016* (pp. 191–201).

Newman, M. (2018). *Networks: An introduction*. Oxford University Press.

Newman, M. E. (2002). Spread of epidemic disease on networks. *Physical Review E*, *66*(1), 016128. https://doi.org/10.1103/physreve.66.016128

Nowak, M. A. (2006). *Evolutionary dynamics: Exploring the equations of life*. Harvard University Press.

Olfati-Saber, R., Fax, J. A., & Murray, R. M. (2007). Consensus and cooperation in networked multi-agent systems. *Proceedings of the IEEE*, *95*(1), 215–233. https://doi.org/10.1109/jproc.2006.887293

Pastor-Satorras, R., & Vespignani, A. (2001). Epidemic spreading in scale-free networks. *Physical Review Letters*, *86*(14), 3200–3203. https://doi.org/10.1103/physrevlett.86.3200

Perelman, L., & Ostfeld, A. (2013). Application of graph theory to sensor placement in water distribution systems. In *Proceedings of world environmental and water resources congress 2013: Showcasing the future* (pp. 617–625).

Riaño-Briceño, G., Sela, L., & Hodges, B. R. (2022). Distributed and vectorized method of characteristics for fast transient simulations in water distribution systems. *Computer-Aided Civil and Infrastructure Engineering*, *37*(2), 163–184. https://doi.org/10.1111/mice.12709

Saleh, S., & Tanyimboh, T. (2014). Optimal design of water distribution systems based on entropy and topology. *Water Resources Management*, *28*(11), 3555–3575. https://doi.org/10.1007/s11269-014-0687-y

Santonastaso, G., Di Nardo, A., Di Natale, M., & Tzatchkov, V. (2020). Pressure management of water distribution networks based on minimum ground elevation difference of DMAS. *Environmental Sciences Proceedings*, *2*, 47. https://doi.org/10.3390/environsciproc2020002047

Schäfer, B., Witthaut, D., Timme, M., & Latora, V. (2018). Dynamically induced cascading failures in power grids. *Nature Communications*, *9*(1), 1975. https://doi.org/10.1038/s41467-018-04287-5

Spizzo, F., Venaruzzo, G., Nicolini, M., & Goi, D. (2023). Water distribution network partitioning based on complex network theory: The Udine case study. *Water*, *15*(8), 1621. https://doi.org/10.3390/w15081621

Starczewska, D., Collins, R., & Boxall, J. (2015). Occurrence of transients in water distribution networks. *Procedia Engineering*, *119*, 1473–1482. https://doi.org/10.1016/j.proeng.2016.01.001

Strogatz, S. H. (2000). From Kuramoto to Crawford: Exploring the onset of synchronization in populations of coupled oscillators. *Physica D: Nonlinear Phenomena*, *143*(1–4), 1–20. https://doi.org/10.1016/s0167-2789(00)00094-4

Szabó, G., & Fáth, G. (2007). Evolutionary games on graphs. *Physics Reports*, *446*(4–6), 97–216. https://doi.org/10.1016/j.physrep.2007.04.004

Torres, J. M., Duenas-Osorio, L., Li, Q., & Yazdani, A. (2017). Exploring topological effects on water distribution system performance using graph theory and statistical models. *Journal of Water Resources Planning and Management*, *143*(1), 04016068. https://doi.org/10.1061/(asce)wr.1943-5452.0000709

Twyman, J. (2018). Water hammer in a pipe network due to a fast valve closure. *Water*, *15*(2), 385.

Vardy, A. (2023). On sources of damping in water-hammer. *Revista Ingeniería de Construcción*, *33*(2), 193–200.

Vesipa, R., & Fellini, S. (2019). Instability of the tank-level control system of water mains in mountainous environments. *Journal of Hydraulic Engineering*, *145*(7), 04019025. https://doi.org/10.1061/(asce)hy.1943-7900.0001609

Xing, L., & Sela, L. (2020). Transient simulations in water distribution networks: Tsnet python package. *Advances in Engineering Software*, *149*, 102884. https://doi.org/10.1016/j.advengsoft.2020.102884

Yazdani, A., & Jeffrey, P. (2012). Applying network theory to quantify the redundancy and structural robustness of water distribution systems. *Journal of Water Resources Planning and Management*, *138*(2), 153–161. https://doi.org/10.1061/(asce)wr.1943-5452.0000159

Yu, X., Wu, Y., Meng, F., Zhou, X., Liu, S., Huang, Y., & Wu, X. (2024). A review of graph and complex network theory in water distribution networks: Mathematical foundation, application and prospects. *Water Research*, *253*, 121238. https://doi.org/10.1016/j.watres.2024.121238